Multidisciplinary Optimization of Shoe Midsole Structures using Swarm Intelligence

Maksudul Alam and Tsz Ho Kwok

Department of Mechanical, Industrial and Aerospace Engineering, Concordia University, 1455 de Maisonneuve Blvd. W., Montreal, H3G 1M8, QC, Canada.

*Corresponding author(s). E-mail(s): tszho.kwok@concordia.ca;

Abstract

Creating functional midsoles for shoes is a challenging task that involves considering different aspects such as stability, comfort, manufacturability, and aesthetics. No single approach exists to design a midsole that meets all these objectives effectively. Therefore, this study aims to introduce a multidisciplinary optimization method to develop custom shoe midsole structures. Our approach involves utilizing generative methods to generate diverse structures and leveraging swarm intelligence to search for optimal designs. Without loss of generality, we use tetrahedral mesh generation to create midsole structures because tetrahedral structures are renowned for their exceptional strength. To enhance the swarm's exploration of the design space and discover more local optima, we developed a swarm behavior that promotes diversity. Furthermore, we created a quantitative measurement tool to evaluate various objectives. In order to test the effectiveness of our generative approach, we analyzed the midsoles generated from our design exploration that performed the best and the worst in relation to each objective. Our findings revealed a substantial difference between them, with scores differing by two to four times. Additionally, when compared to other lattice structures, the tetrahedral midsole structure created by our method demonstrated superior compliance with the foot and better redistribution of plantar stress. The multidisciplinary optimization technique we have proposed is a valuable resource for engineers and designers in the footwear industry, allowing them to develop high-performance midsole structures that meet the needs of both consumers and athletes. Furthermore, this method can be applied to optimize other complex structures in various industries, such as civil, automotive, and aerospace engineering.

Keywords: Multidisciplinary Optimization; Shoe midsole; Swarm Intelligence; Generative Design

1 Introduction

Footwear serves a physiological function for a human being. Wearing appropriate footwear is one of the primary means of maintaining a suitable environment to protect the feet, which bear the weight of the body and are exposed to daily stress. Consumer interest in footwear has expanded beyond durability and appearance to include functional modifications tailored to their individual characteristics. In a shoe, the midsole plays an important role in stabilizing the body, shock-absorbing, energy-absorbing, and cushioning. Using materials, such as polyurethane (PU), ethylene-vinyl acetate (EVA), and polyethylene (PE) foam, in midsoles can alleviate in-shoe pressure. These materials include porosity, which provides lightness and comfort, but the porosity varies depending on the manufacturing method,
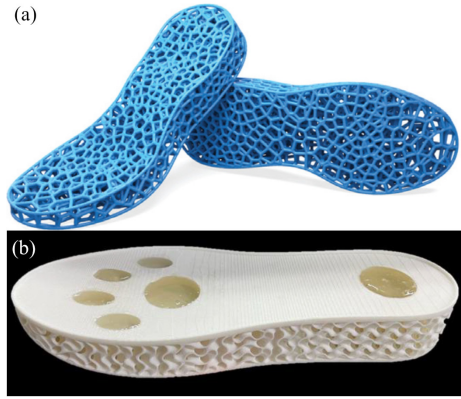
Fig. 1 3D printed midsoles: (a) Voronoi strut midsoles [Cheng et al., 2022], (b) Gyroid lattice midsole [Xiao et al., 2022] © adapted under CC BY-SA 4.0.

and its distribution is extremely difficult to vary. In addition, they have poor breathability and heat transfer properties. However, it is difficult for traditional shoe-making to control the porosity and meet the customization requirements, because of the high cost of customized, complex molds. Three-dimensional (3D) printing has revolutionized the conventional shoe-making process, which has caused the footwear industry to evolve through software and computerized development technologies in speed, efficiency, and customization. 3D-printed shoes can be tailored accurately by changing the modeling data. 3D printing can also fabricate cellular structures, like those in nature [Aguirre et al., 2020], to create lightweight, high performance products. Cellular material's capacity to absorb energy is one of their key qualities [Brennan-Craddock, 2011]. Thus, 3D-printed midsoles (see Fig. 1) are more appealing to customers nowadays. In addition to the necessary stiffness, the shoe midsole needs to have certain elasticity and flexibility; otherwise, it will result in high plantar pressure. High peak plantar pressure is one of the major reasons for painful forefoot syndromes. It is extremely dangerous, even for healthy people [Actis et al., 2008]. Legs, knees, and backs can also be affected because the patients change posture unconsciously to relieve the pain. Along with stress, thermal comfort is another concerning matter. The thermal protection characteristics of footwear play an important role in confining heat inside footwear, particularly in hot environments. As the feet are dense in sweat glands, high temperatures inside the shoe induce

sweating. High levels of foot discomfort from heat and perspiration can happen because of this. However, the shoe sole is the worst heat conductor of a shoe generally [Dessing et al., 2014]. Cellular or lattice structures have many good properties, such as lightweight, high stiffness-to-weight ratio, low thermal expansion coefficient, and high heat dissipation rate [Deshpande et al., 2001b]. Research has shown that the peak plantar pressure of a patient?s feet can be reduced by carefully selecting the lattice cell topology [Cheng et al., 2022]. Using lattice structures in shoe midsoles can also shorten the design cycle and reduce material consumption. However, most research related to midsoles focuses on cushioning and stress relieving, but other aspects, like thermal comfort, aesthetics, and manufacturability, should be considered together too. Unfortunately, seeking globally optimal solutions for multi-objective, non-convex problems can take exponential time with the number of variables. Therefore, there is a need of an effective way for multidisciplinary optimization of midsole structures.

This need motives our research to generate diverse lattice structures for midsoles and search for the best ones as per various objectives. Lattice structures may be categorized into three groups: periodic, conformal, and random [Dong et al., 2017]. The periodic and conformal lattice structures have a repeated pattern of an individual unit cell [Lei et al., 2019]. However, the uniformity nature of these lattice structures often works for simple conditions only. When it comes to complex situations and multiple objectives, applying uniform structures may cause initial geometry to change, geometric continuity to deteriorate, and the inability to adapt to diverse loading circumstances. The struts in a random lattice structure are randomly connected with each other in the design space. This sophisticated topology gives more opportunity to satisfy various objectives simultaneously. Among different kinds of topology, we observe that tetrahedral structures are widely used for their superior strength [Agwu et al., 2021], because they can satisfy Maxwell's criteria of rigidity [Deshpande et al., 2001a]. Being a 3D simplex, tetrahedrons have the capacity to form intricate volumes without constraints on form or topology. Their adaptability and ease of control make them a valuable resource for constructing diverse

2
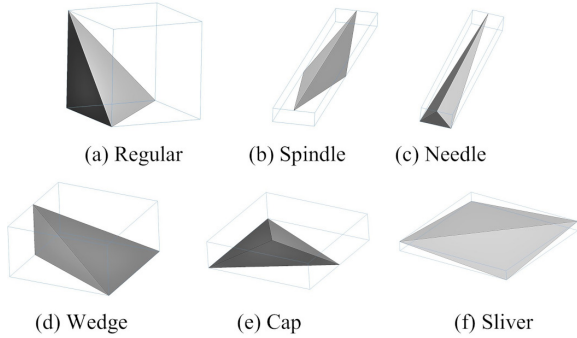
Fig. 2 Tetrahedrons with various aspect ratios.

lattice structures. In addition, the aspect ratio and quality of tetrahedrons (see Fig. 2) can correspond to various properties, including isotropic and anisotropic behavior. Regular tetrahedrons (whose aspect ratio is 1) can be used to create structures that are desired to have isotropic properties [Feng et al., 2021]. Altering the aspect ratio can create a nonuniform, anisotropic, and lightweight structure for shoe midsoles. Many shoes, especially those made for running or other athletic activity, exhibit midsole anisotropy to achieve advanced functions [Sultana et al., 2021]. The combination of these factors renders tetrahedrons a favorable choice for constructing midsole structures. We hypothesize that by altering the shape and size of tetrahedrons within the midsole, a broader range of midsole designs can be achieved. This, in turn, enables the attainment of an optimal equilibrium between strength and flexibility, catering to diverse objectives.

To test this hypothesis, we apply tetrahedral mesh generation to the development of lattice structures for shoe midsoles. Also, by carefully selecting and updating the shape parameters using swarm intelligence, we can generate diverse tetrahedral structures within the design domain. Specifically, the design domain is a 3D volume bounded by the foot scan of a user and the bottom of a shoe. As such, this is a customized domain for the user, and the result will be in total contact with the user's foot. The boundary of the design domain is then served as the input for tetrahedral mesh generation. The tetrahedral properties, such as radius-to-edge ratio, dihedral angle, and volume, are used as the generative parameters to generate tetrahedral meshes with distinct shapes and quality. We thicken the mesh edges to form

cylinders in relation to the specified volume, and thus the connectivity of a tetrahedral mesh forms a lattice structure. To compare the performance of the generated structures, we have defined the quantitative measurement for each of the objectives. For example, minimizing the peak stress to reduce the plantar pressure, maximizing the temperature difference to increase thermal comfort, defining a manufacturing index to measure manufacturability, and developing an aesthetic index based on surveys to consider user preferences. The exploration and searching in the solution space is done by an enhanced version of Particle Swarm Optimization (PSO), which increases the diversity of the locally optimized results. The contributions of this paper are summarized as follows.

- A new framework to optimize custom midsole structure considering multidisciplinary objectives, like stress redistribution, heat dissipation, manufacturability, and aesthetics.
- Applying tetrahedral mesh generation to the construction of midsole lattice structures with distinct properties.
- Enhancing swarm intelligence to the exploration of midsole designs with increased diversity.

The experimental results show that structures produced by the present method exhibit diversity and superior properties compared to other existing lattice structures.

The rest of the paper is organized as follows. Related works are reviewed in Section 2. A detailed discussion of the methodology and the optimization algorithm is given in Section 3. To further validate the proposed method, a case study of a midsole is used, and a comparison between different design configurations as well as experimental analysis is discussed in Section 5. The paper is concluded in Section 6.

2 Literature Review

2.1 Cellular structure modeling

While computer-aided design (CAD) software is employed for modeling various cellular structures, it has limitations in controlling parameters and ensuring design flexibility. To address this, topology and shape optimization approaches have been developed to create intricate structures. Wu *et al.* [Wu et al., 2019] utilized

3
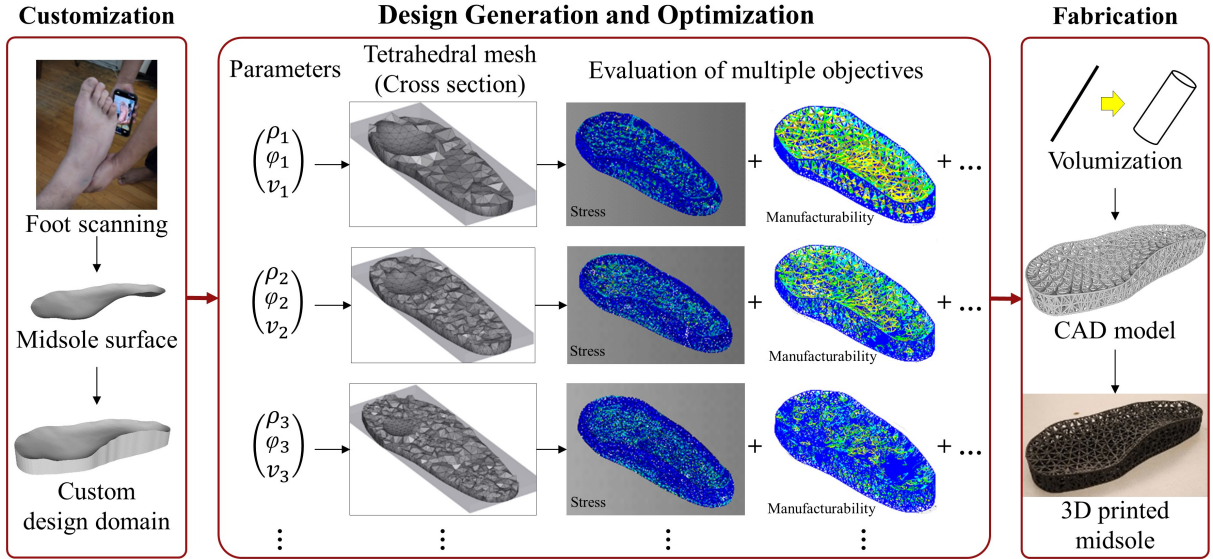
Fig. 3 Overview of the proposed method.

homogenization-based topology optimization and field-aligned parameterization to design lattice structures aligning with principal stress directions and optimized shapes. Panetta *et al.* [Panetta et al., 2015] introduced elastic textures, employing a combinatorial search over topologies followed by shape optimization to achieve diverse isotropic elastic material properties. Martinez *et al.* [Martínez et al., 2017] proposed a meta-material with controllable orthotropic elastic behavior using stochastic and node-connecting algorithms. Watson *et al.* [Watson et al., 2022] presented a parameterization method seamlessly incorporating topology and shape optimization for automated truss system design. In recent years, generative approaches have emerged to overcome CAD software limitations. Classical generative design techniques such as genetic algorithms (GA) [Vaissier et al., 2019], swarm intelligence (SI) [Felkner et al., 2013], cellular automata (CA) [El Bouzouiki et al., 2021], shape grammars (SG) [Zimmermann et al., 2018], and L-systems (LS) [Zhang et al., 2020] use rule-based methods for creating new generations of designs. Bielefeldt *et al.* [Bielefeldt et al., 2019] combined GA and LS for optimizing complex branched structures, while Armanfar *et al.* [Armanfar and Gunpinar, 2022] used a particle tracing algorithm for lattice generation in additive manufacturing. Kwok [Kwok, 2022] utilized

SI to enhance diversity in topology-optimized designs, and El *et al.* [El Bouzouiki et al., 2021] introduced a non-uniform CA algorithm for minimum weight optimization of truss structures. Tomei *et al.* [Tomei et al., 2022] combined SG with GA to minimize the weight of grid shells and diagrid tall buildings. Despite extensive studies in these areas, there is limited research on generative design methods for midsole applications. In this context, this paper focuses on using SI to achieve diversity and the final optimized design.

2.2 Midsole design

Some studies aimed at enhancing midsole performance have explored materials with porosity for lightness and comfort [Muthu and Li, 2021]. However, these materials have limited design freedom, making it challenging to tailor them for specific applications. Lattice structures provide an alternative technique to control midsole performance without altering the materials. Dong *et al.* [Dong et al., 2019] investigated four lattice topologies (diamond, grid, x-shape, and vintile) and found that the lattice topology significantly influences plantar stress, with the diamond lattice performing the best in terms of plantar stress reduction. Zolfagharian *et al.* [Zolfagharian et al., 2021] introduced a design procedure considering body weight

4

index to improve footwear comfort, studying the effects of sole designs on plantar pressure during walking, running, and jumping. Sultana *et al.* [Sultana et al., 2021] assessed the directional energy performance of midsole structures utilizing the lattice's anisotropic property, enhancing energy efficiency when the structure increases energy in the desired direction. However, uniform lattice structures may not meet more complex requirements, leading to the use of partitioning in some designs. For instance, Ali *et al.* [Ali et al., 2020] divided plantar regions based on anatomical characteristics and designed variable-dimension helical springs based on local plantar pressure. Ul Haq *et al.* [ul Haq et al., 2022] proposed a multifunctional shoe midsole design method incorporating functionally gradient wave springs at critical foot pressure areas and gradient cellular structures in non-critical areas. Wang *et al.* [Wang et al., 2021] used alternating gradient lattice structures for shoes, demonstrating better cushioning performance than uniform lattice structures. Despite these benefits, weak sections can arise at boundaries between partitions, prone to breakage during wear. To address these challenges, a widely used approach involves generating lattice structures for the entire domain using Voronoi diagrams. Bugun *et al.* [Bugin et al., 2020] used Grasshopper, a commercial software plug-in, to combine biomechanical data with 3D Voronoi diagrams for variable density midsoles. Cheng *et al.* [Cheng et al., 2022] proposed a Voronoi strut midsole structural design method driven by plantar pressure distribution, evaluating mechanical and cushioning performance. Beyond plantar pressure, thermal properties play a crucial role in footwear comfort. Dessing *et al.* [Dessing et al., 2014] conducted experimental research on shoe ventilation properties, identifying the sole as the worst heat conductor. Some research focuses on shoe materials [Yick et al., 2019], with textile-fabricated insoles showing no significant changes in foot skin temperature compared to other materials [Ning et al., 2022]. Thermal analysis models have been developed to evaluate the thermal effects of shoe sole internal heat generation on foot comfort [Shimazaki and Aisaka, 2018]. While there are works fulfilling customers' semantic needs [Lee and Han, 2022] and customizing shoes using total contact inserts [Tang et al., 2021], none have considered all factors together in the design and optimization of shoe midsoles.

3 Methodology

Figure 3 shows an overview of the present method. To achieve total contact in a custom shoe sole, the input is obtained by scanning the bottom surface of a foot. This defines the upper surface of the design domain for the midsole, which is then used to generate various lattice structures. The generation process employs a diversity-enhanced particle swarm optimization technique. Subsequently, the generated structures are evaluated based on a combined metric that considers multiple objectives. Technical details for each of these steps are provided in the following subsections.

3.1 Design Domain for Custom Midsole

To create a customized midsole design for each user, we begin by using the Foot ID app [KevinRoot Medical,] on an iPhone 13 to perform a detailed 3D scan of their foot. This app utilizes the TrueDepth camera system, which includes sensors, cameras, and a dot projector, to capture both infrared images and dots. This data is then fed into neural networks, which generate a precise mathematical model of the foot. Next, we extract only the bottom surface of the reconstructed foot and use it as the input for our framework. We align the scan surface with the $x - y$ plane at a user-specified height, assuming the $x - y$ plane at $z = 0$ is the ground. Although the bottom of the shoe can be of any shape, we assume it to be flat for simplicity. The bottom surface of the design domain is obtained by projecting the scan surface onto the ground. We then connect the top and bottom surfaces with a strip at their boundary to define a closed volume for the design domain. Finally, we perform a uniform remeshing that preserves sharp edges to prepare a proper triangular mesh for the next step.
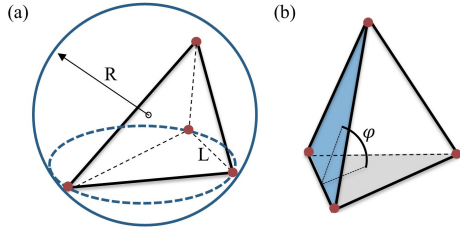
Fig. 4 (a) The radius-to-edge ratio (R/L) and (b) the dihedral angle (φ) of a tetrahedron.

3.2 Generative Parameters for Lattice Generation

The present method uses tetrahedral mesh generation to construct lattice structures and explores diverse solutions based on a set of input parameters, so it is important to set up these parameters properly. The process of generating tetrahedral meshes in this paper is carried out using TetGen, an open-source program [Hang, 2015]. A variety of parameters are available within the program to govern the mesh generation process, such as input mesh preservation, maximum radius-to-edge ratio, minimum and maximum dihedral angles, maximum volume, mesh coarsening, mesh refinement, level of mesh optimization, adding additional points. While utilizing more parameters can yield a greater range of results, it also exponentially increases the computation time. Consequently, we have chosen to focus on the most important and influential parameters in order to generate tetrahedrons with distinct shapes and characteristics.

First, the radius-to-edge ratio (ρ) of a tetrahedron is the ratio between the radius R of its circumscribed sphere and the length L of its shortest edge, i.e., $\rho = R/L$, as depicted in Fig. 4a. For instance, a regular tetrahedron typically has a ratio of around 0.6, while a cap tetrahedron may possess a ratio larger than 2.0. Therefore, the radius-to-edge ratio represents a significant shape factor, and we utilize the maximum radius-to-edge ratio (ρ_{max}) as one of the controlling parameters. Regulating solely the maximum value of the ratio implies that certain tetrahedrons may have a lower ratio if it is the only way to meet other criteria. While an excessively low maximum ratio results in limited options for available shapes to occupy the design domain, and could lead to mesh generation failure, a very high ratio should also be avoided. Overly lenient constraints are, in essence, comparable to having no restrictions, resulting

in identical outcomes. Based on our preliminary analysis of the parameter (see Appendix A), the effective range is from 1.15 to 1.6.

Second, the dihedral angle (φ) is the angle between two faces of a tetrahedron and varies between 0° and 180°. Just like how the interior angles of a triangle are interdependent, the dihedral angles of a tetrahedron also influence one another. When some of them are very large, the remaining angles must be very small, such as in a silver tetrahedron. Regular tetrahedrons have dihedral angles ranging from 60° to 90°. Therefore, the dihedral angle is another shape factor that has a direct relationship with the tetrahedral shapes. Since the dihedral angles are interrelated, we only need to regulate either the minimum or maximum dihedral angle to achieve various shapes. In this study, we choose to control the minimum dihedral angle (φ_{min}) and set its range from 0° to 18°, based on our preliminary analysis.

Third, each tetrahedron takes up a specific volume within the design domain, and as the size of the tetrahedrons decreases, more of them are needed to fill the entire domain. This, in turn, has a direct impact on the number of struts in the lattice structure and its level of topological complexity. To regulate this effect, we set the maximum volume of tetrahedrons (V_{max}) within the range of 1000 mm^3 to 7000 mm^3.

We either use the default values of the program or apply values that do not conflict with other parameters for the remaining parameters. The table below summarizes the selected generative parameters and their range for obtaining diverse results. Additionally, all other parameters are listed.

Table 1 List of generative parameters and other parameters.

Parameters	Range/Value
Max. radius-to-edge ratio (ρ_{max})	1.15 to 1.6
Min. dihedral angle (φ_{min})	0° to 18°
Max. volume (V_{max})	1000 to 7000 mm^3
Max. dihedral angle	165°
Mesh Refinement	On
Mesh Coarsening	Off
Input Mesh Preservation	No

3.3 Diversity-Enhanced Particle Swarm Optimization

The fundamental principle behind the particle swarm optimization (PSO) algorithm involves the movement of a group of particles within a search space, where each particle represents a potential solution. The particles' movements are influenced by both their individual best-known position within the search space and the overall best-known position of the entire swarm. The calculation of their velocity can be expressed as follows.

$$\mathbf{V_i} = w\mathbf{V_i} + c_1 r_1(\mathbf{P_i} - \mathbf{X_i}) + c_2 r_2(\mathbf{S} - \mathbf{X_i}), \quad (1)$$

where V_i is the velocity of particle i, w is the inertia coefficient (e.g., 1), $\mathbf{P_i}$ and $\mathbf{S}$ are the particle's and the swarm's best-known positions, $\mathbf{X_i}$ is the particle's current position, c_1 and c_2 are the local and global acceleration coefficients (e.g., 2), and r_1 and r_2 are randomly generated numbers in the range $[0, 1]$. Then, the particle's position is updated by the velocity.

$$\mathbf{X_i} = \mathbf{X_i} + \mathbf{V_i} \quad (2)$$

This process is repeated iteratively in order to explore potential solutions and ultimately aim to discover a satisfactory solution. The PSO algorithm can be conceptualized as having three components guiding the particles' movement: an inertia component, a cognitive component, and a social component. The inertia component is the tendency to move in the same direction. The cognitive component reflects each particle's individual memory of its best-known solution ($\mathbf{P_i}$), encouraging exploitation by directing the particle towards its own best solution in the search space. The social component reflects the swarm's collective memory of the best-known solution ($\mathbf{S}$), encouraging exploration by directing the particle towards the best solution found by the entire swarm. As the particles move towards the overall best solution, they tend to converge towards a single solution, which allows them to escape from local optima and continue to search for better solutions. It is assumed that better solutions are located in the direction of the swarm's best position. However, if the initial positions of the particles are far from the global optimum, it may be challenging to discover it.

Our argument is that when the neighboring particles of the swarm's best position are functioning adequately, other particles should not move towards this position. Rather, they should prioritize enhancing diversity and exploring various local optima to maximize the probability of discovering the global optimum. Hence, we expect the particles to exhibit the following behaviors:

Local search: They find the best solution for the region where they are located.
Migration: Once they complete searching a local region, they explore other local optima.
Division: They prevent redundant efforts by avoiding searching the same region.

To achieve these behaviors, we have implemented the following modifications to the algorithm. Firstly, we removed the consideration of the swarm's best position ($\mathbf{S}$) and added a neighborhood factor to the social component. The velocity equation (Eq. 1) then becomes:

$$\mathbf{V_i} = w\mathbf{V_i} + c_1 r_1(\mathbf{P_i} - \mathbf{X_i}) + c_2 r_2(\mathbf{N_i} - \mathbf{X_i}), \quad (3)$$

where $\mathbf{N_i}$ denotes a neighboring position of $\mathbf{X_i}$, and c_2 is now a neighboring coefficient. Secondly, we made a particle focus on searching its local region by eliminating the social component's influence. This is done by setting c_2 to 0, which causes the particle to move solely according to the cognitive component, thereby looping around its best position due to inertia. Thirdly, when a particle is unable to discover better solutions after five local searches, we assign a negative coefficient to the cognitive component ($c_1 = -2$) to move the particle out of the local region and explore other areas. This process stops when the particle finds a better solution, after which it switches back to the local search. Finally, during migration, if a particle is in close proximity (2% of the search space size) to an explored region, we steer it away from that direction by setting c_2 to -2 and $\mathbf{N_i}$ to the closest explored position. To summarize, the coefficients are established based on the expected behaviors as follows.

$$w, c_1, c_2 = \begin{cases} 1, 2, 0 & \text{for local search} \\ 1, -2, 0 & \text{for migration} \\ 1, 0, -2 & \text{for division.} \end{cases} \quad (4)$$
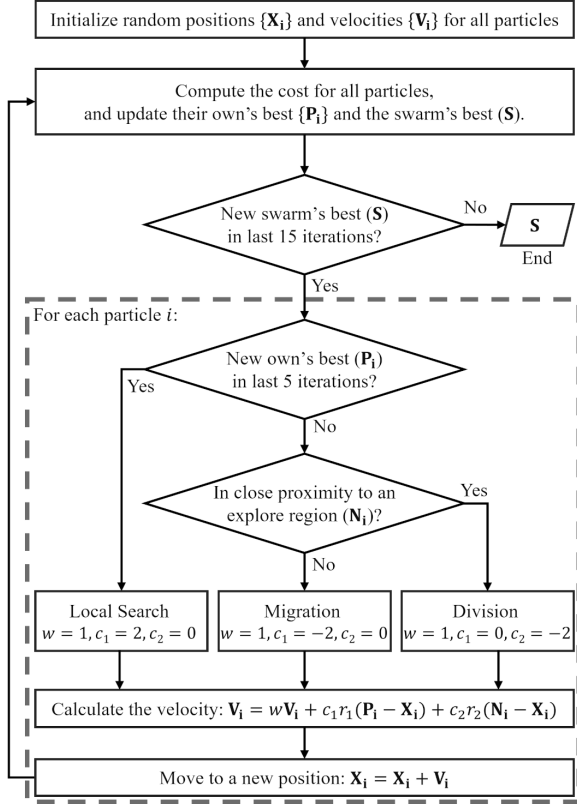
Fig. 5 The flowchart of the multidisciplinary optimization framework.

The flowchart of the diversity-enhanced PSO algorithm is depicted in Fig. 5.

4 Quantitative Measurement of Objectives

In the previous section, we discussed the generative approach to creating diverse designs. However, to optimize the designs, we need a quantitative method of measurement to efficiently determine which designs are better. This section aims to develop a measurement for each objective. The paper considers four objectives: plantar stress (O_S), heat dissipation (O_H), manufacturability (O_M), and aesthetics (O_A). The optimization's cost function is the weighted sum of all objectives, i.e.,

$$cost = w_1 O_S + w_2 O_H + w_3 O_M + w_4 O_A \quad (5)$$

The user can set the weights of the objectives according to their preferences, or they can use the default equally weighted values, where $w_1 = w_2 = w_3 = w_4 = 0.25$. The main challenge in optimizing the designs is how to quantify the objectives. The following subsections provide a detailed description of each objective.

4.1 Plantar Stress Redistribution

Discomfort and health issues, especially for diabetic patients, can be caused by high plantar stresses. Therefore, a midsole should be designed to reduce these high pressures and provide accommodative support. Since the user's weight cannot be changed, most studies focus on redistributing the plantar stresses to achieve uniform stress distribution throughout the foot. This means reducing the peak stress as much as possible and bringing it closer to the average stress. Although direct measurement of peak normal stress at the bottom surface of the foot is a common approach to achieve this objective, this paper chooses to minimize the maximum stress of the midsole for the following reasons. Firstly, the forces applied by the foot on the midsole and the forces exerted by the midsole on the foot are a pair of action and reaction forces. When the stresses in the midsole are distributed evenly, these forces are also uniformly distributed. Secondly, reducing the maximum stress on the midsole structure for the same applied loads indicates that the structure is more robust and can withstand higher loads without failure. Thirdly, it is worth mentioning that many foams and plastics exhibit hyperelastic behavior, whereby stress increases exponentially after the strain surpasses a certain threshold. By reducing the maximum stress, the midsole can undergo greater deformation and maintain full contact with the foot, thus avoiding stress concentration.

To obtain information about the maximum stress (S_{max}), we used MatLab to script the Ansys Parametric Design Language (APDL) to run the Ansys Mechanical solver. In the simulation model, each strut of the lattice structure is represented by a one-dimensional (1D) beam element. This idealization significantly reduces computation time. The loading and boundary conditions are shown in Fig. 6. The bottom surface, assumed to be in contact with the ground, has a fixed boundary
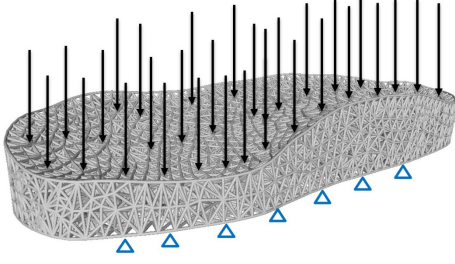
Fig. 6 Applied conditions for mechanical analysis.
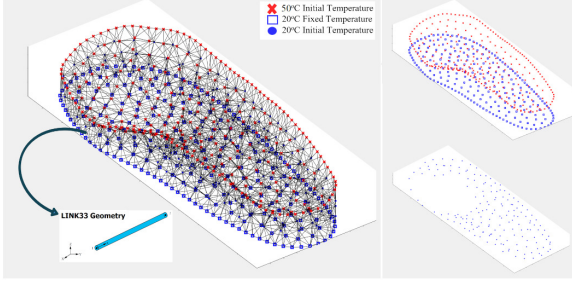
Fig. 7 Applied conditions for thermal analysis.

condition, while a downward load, simulating a foot stepping on it, is applied to the top surface. Previous research [Nandikolla et al., 2017] indicated that the reaction force in jumping is about three times higher than one's weight. Therefore, we set the load as 240 kg evenly distributed across the entire top surface.

Since the maximum stress (S_{max}) could have a unit of megapascal, which is a large value of 10^6, adding it directly to the cost function may significantly affect the optimization. To avoid biasing the optimization towards the maximum stress objective, we need to normalize the scale among all objectives. Here, we take the reference from the tensile strength (TS) of the material and use a safety factor of 0.5 to obtain a normalization factor. We divide the maximum stress by this normalization factor to obtain the normalized objective function, which is expressed as

$$O_S = \frac{S_{max}}{0.5TS}.$$

4.2 Heat Dissipation

According to [Kinoshita and Bates, 1996], a foot wearing a shoe can become as hot as 50°C during exercise, making it crucial for a shoe to dissipate
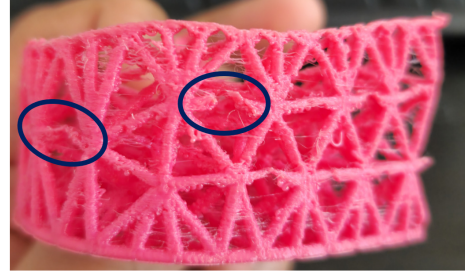
Fig. 8 Manufacturing defects by FFF 3D printing.

heat effectively to prevent discomfort. To assess a shoe's heat dissipation ability, we conducted a thermal analysis with the boundary conditions depicted in Fig. 7. The top surface's initial temperature is set to 50°C to simulate the foot's temperature, while the bottom surface's temperature remains fixed at 20°C, assuming it is in contact with the ground. All other nodes' initial temperature is 20°C.

Similar to the mechanical analysis, the transient thermal analysis employs Ansys APDL, and each strut uses the LINK33 element. To simplify the analysis, we only consider thermal conduction since free convection heat transfer has a negligible effect. As the top surface's temperature decreases over time, the midsole structure removes heat from the foot more efficiently, improving foot comfort. Therefore, we aim to minimize the highest temperature (T_{max}) on the upper surface after a fixed time duration, which we set to 10 seconds in this paper. To balance the scaling effect among different objectives, the temperature value is normalized by using the given highest temperature (T_h), which is 50°C and the skin temperature (T_{skin}) which is 37°C [Rebay et al., 2007]. The objective function is defined as

$$O_H = \frac{T_{max} - T_{skin}}{T_h - T_{skin}}.$$

4.3 Manufacturability

Ensuring manufacturability is crucial in achieving a successful design, as any manufacturing defects (as shown in Fig. 8) can impede the product's intended functionality. In the case of 3D printing the shoe midsole using fused filament fabrication (FFF), it is important to consider the limitations of this method [Dong et al., 2018, Guerra Silva et al., 2021,

Beloshenko et al., 2021]. Strut length and overhang angle are critical factors that affect print success, and we have defined a manufacturing index to quantify the manufacturability of a lattice structure based on its geometry. Short struts can be printed at any angle due to bridging, and struts with an overhang angle less than a certain angle can be printed regardless of their length, as they are self-supporting. For longer struts, print quality depends on both length and overhang angle, requiring consideration of both factors to determine manufacturability. A score can be assigned to a lattice structure to provide a measure of its manufacturability, taking all these factors into account. However, these geometric factors are not universal, and they are also dependent on the printing material, printer, and process parameters. Assuming that the same material, printer, and settings will be used, a trial print can be conducted with struts of varying lengths and overhang angles to update the thresholds for calculating the manufacturing index.

For instance, by employing an Ultimaker 3 with print height of 0.1 mm, print speed of 12 mm/s, print temperature of $225°C$, and 100% infill, we established the strut length threshold (L_{max}) to be 5 mm and the overhang angle (θ_o) threshold to be $45°$. Next, we assign a manufacturing score (M), between 0 and 1, to each strut (s) based on its length (L) and overhang angle (θ) using the following approach:

$$M(s) = \begin{cases} 1, & \text{if } L < L_{max} \text{ or } \theta < \theta_o \\ \frac{1}{2}(\frac{L_{max}}{L} + \frac{90° - \theta}{\theta_o}), & \text{otherwise} \end{cases}$$

The first scenario has a score of 1, indicating that the print is always successful. The second scenario consists of two components. The first component is a measure of how much longer the strut is than the length threshold, resulting in a lower value for longer struts. The second component is a measure of how much larger the overhang angle is than the angle threshold, with a maximum angle of $90°$. A lower value is assigned to larger angles. Both components have a range of 0 to 1, and a factor of $\frac{1}{2}$ is multiplied to generate a score ranging from 0 to 1. The manufacturing index of a structure is computed by taking the average score of all its struts and subtracting it from one, as

a higher score implies better performance. However, the manufacturing index does not start at zero since even the worst strut has some good struts nearby. For example, in a typical joint with six struts, two of them might have a score of 0 due to their length and horizontal orientation, but the other four should still have high scores. To address the scaling effect, the manufacturing index is normalized further by dividing it by 0.34:

$$O_M = \frac{1}{0.34}\left(1 - \frac{1}{|s|}\sum_s M(s)\right)$$

4.4 Aesthetics

Design aesthetics play a critical role in influencing consumer purchasing decisions. However, quantifying and measuring them remains a challenging task. In this regard, we conducted a survey to investigate some visual design factors for tetrahedral midsoles. However, it is important to note that our goal is not to develop a comprehensive method for aesthetic measurement in this paper. In the survey, 54 participants were asked to rank several midsole structures on a scale of 1 to 5 based on their aesthetic preferences. Participants rated how much they liked the midsoles as a potential customer. The midsole they liked the most was ranked as 1, and the least favorite was ranked as 5. At the time of designing the survey, we were unsure of the important factors. Therefore, we selected five tetrahedral midsoles based on the difference in mesh size. The midsoles and their corresponding rank distribution are depicted in Fig. 9. Although the survey results indicate that people have diverse preferences, one particular rank stands out for each midsole. Specifically, midsole A is ranked first, followed by midsole C, midsole D, midsole E, and finally midsole B. Upon further discussions with some of the participants, we discovered that they commonly considered two factors: structure density and uniformity. Participants tended to favor a coarse structure over a dense one, and they found that midsoles with more uniformity were more visually appealing.

For better comparability, we have presented the structure statistics of the midsoles in Table 2 according to their respective rankings. We use the number of joints to provide an indication of structure density, as a higher number of joints implies a denser structure. Also, we employ the
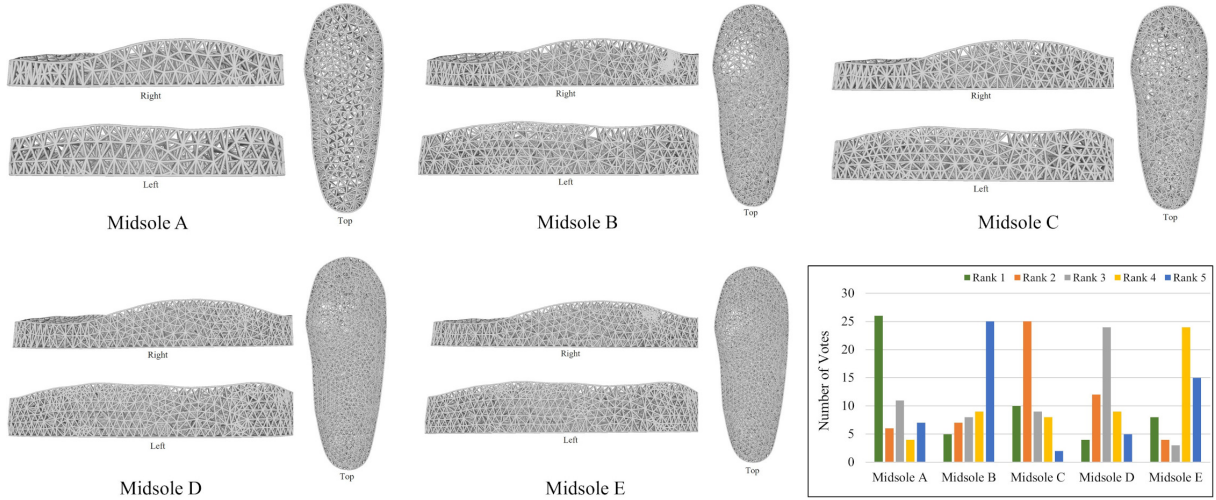
Fig. 9 Different midsole structures considered in the survey and the ranking result.

Table 2 Structure statistics of the midsoles in the survey, including the number of joints (#Joint) and the mean, the standard deviation (Std), and the percentage within 1 std from the mean (Std_1) of the strut length.

Midsole	Rank	#Joint	Strut Length		
			Mean	**Std**	**Std$_1$**
A	1	648	12.11	4.50	72%
C	2	1190	9.23	2.69	64%
D	3	3153	6.14	2.14	67%
E	4	3593	5.80	2.10	68%
B	5	2369	6.27	3.21	61%

percentage of strut lengths within one standard deviation (std) from the mean to denote the uniformity of the structure. A more uniform structure should have a higher percentage within the one std range (Std_1). As shown in the table, the ranking is strongly correlated with the number of joints, with the exception of midsole B. Despite having fewer joints (2369) than midsoles D (3153) and E (3593), midsole B has the lowest uniformity (61%) and is ranked last. Midsole A has the lowest number of joints (648) and the highest level of uniformity (72%), making it the top-ranking midsole. To measure aesthetics for tetrahedral midsole structures, we use the two data of #Joint and Std_1, as they showed a good alignment with the survey ranking. To normalize the Std_1 part, we use the value of one minus Std_1 and divide it by 0.32. This will normalize the value to more or less than one compared to the Std_1 of normally distributed data. To normalize the #Joint, we take the reference of the input mesh size ($\mathbf{I}$), i.e., the foot scan. As the tetrahedral mesh must have a larger size than the input surface mesh, we multiply the input mesh size by 5 to obtain the normalization factor. The objective function is defined as the average of the two values:

$$O_A = 0.5 \left(\frac{\#Joint}{5|\mathbf{I}|} + \frac{1 - Std_1}{0.32} \right)$$

5 Results

The proposed method was implemented using Matlab on a PC with an Intel Core i5 6500 3.2 GHz processor and 16 GB memory. A solid-to-void ratio of 0.3 was established for the design domain, meaning that for denser structures, the struts were made thinner to ensure that all designs contained the same quantity of material. The material considered in this study is Ice9 Flex, produced by TCPoly (Atlanta, GA, USA), which is a flexible material that is used for shoe midsoles because of its high elasticity and thermal conductivity. The relevant material properties are listed in Table 3. However, this material utilized throughout our project has been exhausted and is presently unavailable from local vendors. Regrettably, at the time of writing this paper, we were unable to procure more. Despite having to use alternative materials to construct the designs that were originally intended for this material, the validation has not been compromised. These materials
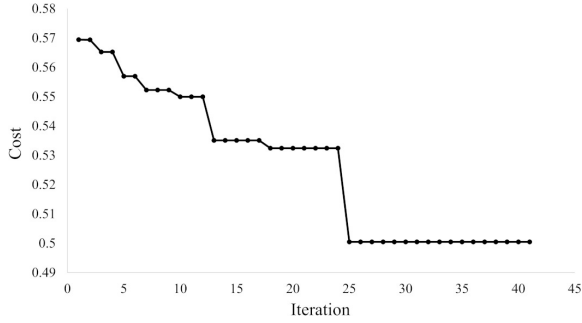
Fig. 10 Convergence curve of the PSO optimization.
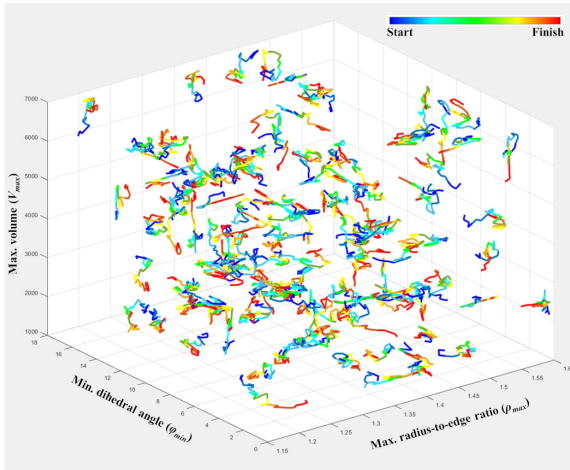
Fig. 11 Trajectory of particles in the search space.

are the thermoplastic polyurethane (TPU), produced by Ninjatek (Lititz, PA, USA), and the polylactic acid (PLA), produced by Filaments.ca (Mississauga, ON, Canada). Their properties are also included in Table 3.

Table 3 Material properties of Ice9 Flex, TPU, and PLA.

Property	Ice9	TPU	PLA
Density (kg/m^3)	1400	1100	1240
Therm conduct (W/m-K)	8	0.15	0.13
Specific heat (J/kg-K)	1300	1210	1700
Elastic modulus (MPa)	95	12	2400
Tensile strength (MPa)	15	26	48
Shore hardness	88A	85A	70D

The optimization process involved randomly distributing 100 particles within the search space, with each particle initialized with a random velocity. The cost function for a given structure was computed in under a minute, and optimization converged after 41 iterations, during which the global best remained unchanged for 15 iterations (see Fig. 10). The convergence curve shows several small drops, indicating effective local search, and large drops, indicating the discovery of new optima. Figure 11 shows the particles' trajectories over the iterations, revealing that each particle focused on a specific region of the search space to maximize the chances of finding more optima. The twisted parts of the trajectory correspond to local optimization, while the extended parts indicate the particles' attempts to locate better local bests outside their current vicinity.

5.1 Validation of Generative Method

In this paper, a generative approach is proposed to achieve a wide variety of designs and thus increase the chances of finding the global optimal solution. To verify the efficacy of this method, we examine the best and worse designs for each objective among all the generated outcomes (refer to Fig. 12). This validation aims to assess whether the approach can truly generate diverse designs concerning the objectives.

To begin with, there is a significant difference between the maximum stress values of the best and worst structures for the planter stress objective (O_S). Specifically, the best structure has a maximum stress of 3.08 MPa, whereas the worst one has a much higher maximum stress of 7.46 MPa – more than twice as high as that of the optimal structure. In terms of heat dissipation (O_H), the most effective structure reduces the temperature at the top surface by 10.6°C, from 50°C to 39.4°C. In contrast, the least effective structure only lowers the temperature by 2.5°C, resulting in a top surface temperature of 47.5°C. In other words, the optimal structure is four times more efficient in dissipating heat than the worst performing structure. Furthermore, the third column of Fig. 12 displays a color map that represents the manufacturing scores of the struts, with blue indicating good scores and red indicating poor scores. It should be noted that the manufacturing index (O_M) has an inverse relationship with the manufacturing score ($M(s)$). The best structure has a manufacturing index of 0.25,

12
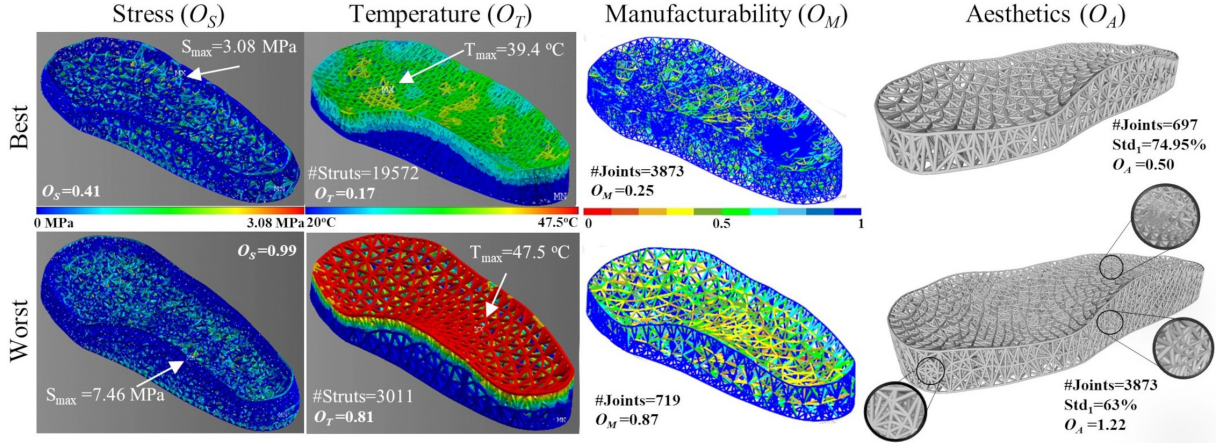
Fig. 12 The best and the worst structures for each of the objectives separately.
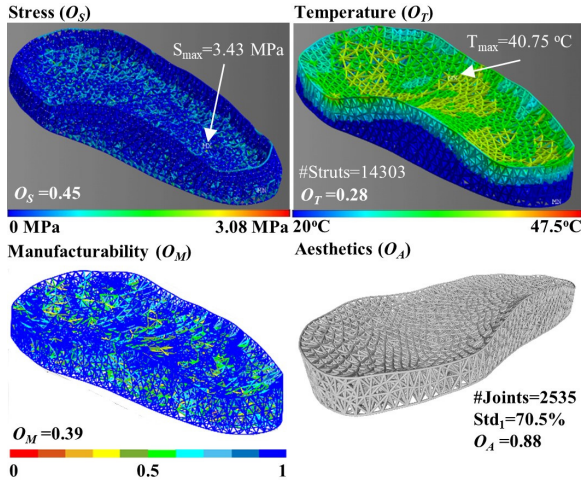
Fig. 13 The overall best structure of combined objectives.

while the worst structure has a significantly higher index of 0.87 – a difference of 3.5 times between the two. Lastly, the aesthetics objective function (O_A) considers both the density and uniformity of a structure, with a lower value indicating higher aesthetic appeal. The optimal structure according to this function has a small number of joints (697) and a Std_1 value of 74.95%, resulting in an O_A score of 0.50. On the other hand, the least appealing structure has almost five times as many joints (3,873), looks dense, has a Std_1 value of 63%, and contains some non-uniform regions that are highlighted with zoom-in views. Its aesthetics index is 1.22, which is around 2.5 times higher than that of the best structure.

To summarize, despite the optimization being targeted at the combined metric of all objectives, the generated solutions demonstrate varying levels of performance from the perspective of each individual objective. This confirms the success of the generative method, which uses tetrahedral mesh generation and diversity-enhanced swarm intelligence, in generating a range of diverse designs. Furthermore, the best structures for each objective are vastly different, with the best structure for heat dissipation being a densely packed one, while the best aesthetics-focused structure being a more coarse one. Therefore, a trade-off must be made via a multi-objective optimization process. The structure that performs the best overall for the combined metric is illustrated in Fig. 13. It demonstrates superior performance for most objectives, with $O_S = 0.45$ (the best O_S being 0.41), $O_T = 0.28$ (the best O_T being 0.17), $O_M = 0.39$ (the best O_M being 0.25), and $O_A = 0.88$ (the best O_A being 0.50). The differences between the maximum stress (S_{max}) and maximum temperature (T_{max}) of this structure and the corresponding best structures are only 10% and 3%, respectively. The aesthetics performance is the most compromised objective in this structure, mostly because a denser mesh is required to enhance other performances. Overall, this structure maintains a satisfactory balance between all objectives, proving the effectiveness of the proposed optimization approach.
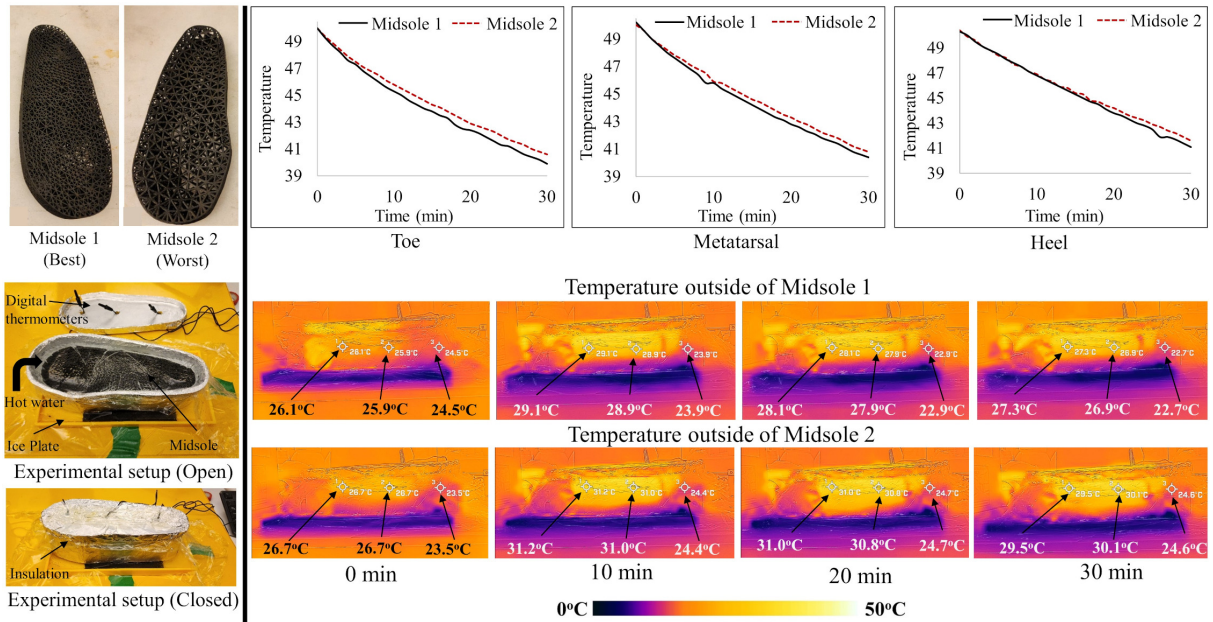
Fig. 14 Thermal experimental setup for the best (Midsole 1) and worst (Midsole 2) structures of thermal performance. The results include the temperature sensor data in the toe, metatarsal, and heel zones, as well as the thermal images at various time instants.

5.2 Thermal Validation

We fabricated the best and worst structures of thermal performance (second column of Fig. 12) to validate the quantitative measurement of heat dissipation. These midsoles were subjected to a thermal experiment. However, due to the unavailability of the Ice9 material, we printed the midsoles using the PLA material. The thermal conductivity of PLA (0.13 w/mK) is much lower than Ice9 (8 w/mK). However, improvements in a low thermal-conductive material can lead to even greater improvements in a higher thermal-conductive material. The midsoles we fabricated are shown in Fig. 14, with midsole 1 being the best and midsole 2 being the worst. Both midsoles were weighed to ensure that they had the same amount of material. To prevent thermal convection from causing heat loss, we wrapped the midsoles in insulators made of plastic wrap and aluminum foil. The bottom of the midsoles was in contact with cool water at 10°C, while the volume on top of the midsoles was filled with hot water at 50°C. The volume was approximately 750 ml, similar to the volume occupied by a foot. To prevent the water from leaking, a thin plastic film was placed between the water and the midsole. We recorded the temperature at the heel zone, metatarsal zone, and toe zone every minute for 30 minutes using three Amropi aquarium thermometers. Additionally, we used a FLIR ONE Pro thermal camera, manufactured by Teledyne Flir (Wilsonville, OR, USA), to capture temperature changes from the outside.

Figure 14 shows the results of the experiment. The thermometer data is presented in curves, and thermal images were taken at 0 min, 10 min, 20 min, and 30 min. The plots reveal that the water temperatures decrease over time, but the rate of temperature change is greater in midsole 1 than midsole 2. After 30 minutes, the temperature differences between midsole 1 and midsole 2 in the toe, metatarsal, and heel zones are 0.7°C, 0.4°C, and 0.5°C, respectively. Although the differences are not significant due to the low thermal conductivity of the PLA material, human skin is highly sensitive to temperature changes and can detect differences as low as 0.03°C [Jones, 2009]. Therefore, midsole 1 can dissipate more heat from the top surface than midsole 2, with the same amount of material. The thermal images are consistent with the sensor data. Additionally, three points were chosen at the water-midsole interface for
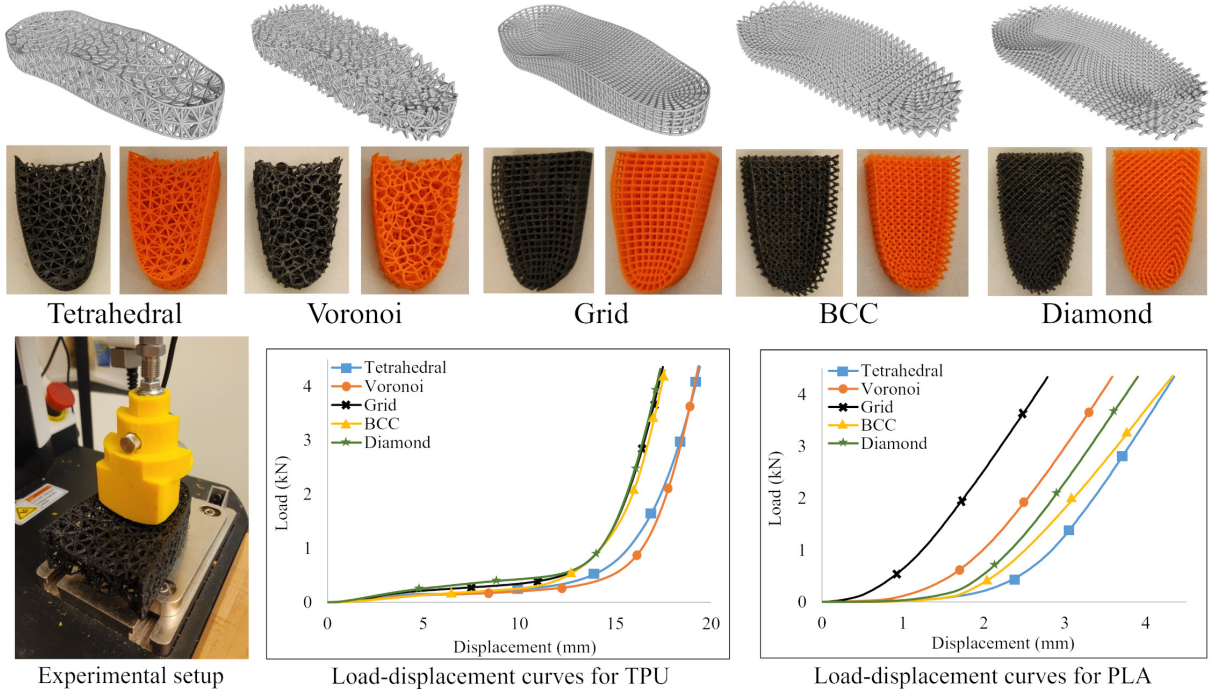
Fig. 15 Compression tests on tetrahedral, Voronoi, grid, body centered cubic (BCC), and diamond structures, printed in both TPU and PLA materials. The results are shown in the load-displacement curves.

comparison, and they remained fixed throughout the experiment. At the start (0 min), the outside temperatures were close to room temperature and increased as the hot water was added. Thereafter, they decreased in sync with the water temperatures. For example, the leftmost point in midsole 1 had a temperature of 29.3°C at 10 min, 28.1°C at 20 min, and 27.3°C at 30 min. Conversely, the same point in midsole 2 had higher temperatures of 31.2°C at 10 min, 31.0°C at 20 min, and 29.5°C at 30 min. The results of this experiment confirm that our quantitative measurement for heat dissipation is accurate and effective.

5.3 Comparison with Other Lattices

Other lattice shoe soles have been described in the literature [Dong et al., 2019, Cheng et al., 2022]. In order to compare the tetrahedral lattice structure generated by our method with other structures, we conducted compression tests to determine their mechanical responses. The best performing structure in plantar stress redistribution (best O_S in Fig. 12) was chosen, and other lattices, including grid, body centered cubic (BCC),

diamond, and Voronoi structures, were evaluated and are shown in Fig. 15. The grid and BCC structures are relatively simple and regular, serving as a baseline for comparison. Diamond is known to be strong and has a tetrahedral-like structure, with each joint having four neighboring joints. It can be viewed as a specific case of our results, as it is a uniform tetrahedral lattice. The Voronoi lattice is random and highly structurally complex, similar to the tetrahedral lattice. In fact, a Delaunay tetrahedralization is the dual of a Voronoi diagram. However, the connectivity and properties of the Voronoi structure are completely different due to its basic element being a polyhedron. To ensure a fair comparison, all midsoles were designed with the same weight and strut diameter, but differed in connectivity and number of struts. It is worth noting that while these structures are known for their good structural performance, none of them can be considered optimized within the context of this study.

They were tested with both PLA and TPU to assess their performance in rigid and soft materials, respectively. The elasticity moduli of PLA and TPU are 2400 MPa and 12 MPa, respectively.

The inclusion of PLA samples is to emphasize their linear behavior, serving as a sanity check. This helps to ensure that the structure is sound by demonstrating a similar trend to elastic materials. By doing so, we can verify the consistency and reliability of the structural performance, as the linear behavior of PLA provides a clear and straightforward benchmark against which we can compare the more complex behavior of TPU. This comparison confirms that the structural response aligns with expected patterns, thereby validating our approach. Since the testing was limited to the heel zone, only half of the midsoles were printed, and their weights were carefully measured to ensure equal amounts of material were used. A press-head was designed based on the surface of the heel zone and fabricated in PLA. The midsole samples were placed on a compression plate, and the press-head was used to apply a uniaxial compression load. The Mark-10 ESM750SLC universal testing machine was used for the experiment, with a strain rate of 10 mm/min.

The load-displacement curves were used to plot the testing results. In the case of TPU, the curves show little difference initially due to the softness of the material, but they diverge into two groups when the deformation is large. The first group, consisting of the grid, BCC, and diamond structures, exhibit a rapid increase in load at a smaller displacement than the second group, which includes the tetrahedral and Voronoi structures. This increase is due to the densification of the lattices, and the tetrahedral and Voronoi structures allow more deformation before densification, resulting in better contact with the foot and less stress concentration. Looking at the load-displacement curves for PLA, the structures' differences are more apparent, with stiffness in the following order: grid, Voronoi, diamond, BCC, and tetrahedral structures. The load measured by the load cell above the press-head can be viewed as the reaction force applied to the foot by the midsole. When this force is higher at the same displacement, it results in higher foot plantar pressure. The tetrahedral lattice structure exhibits greater compliance with the foot and better redistribution of plantar stress, making it an excellent choice for use in shoe midsoles.
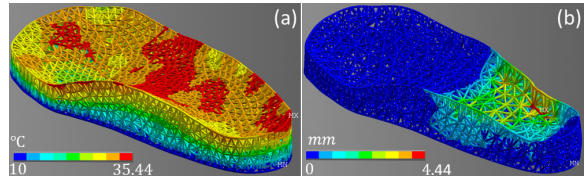
Fig. 16 (a) Simulated temperature map for midsole 1 from Fig. 14. (b) Simulated deformation for the PLA tetrahedral midsole from Fig. 15.

5.4 Discussion: Simulation and Experimental Results

In general, it is important to validate simulation results with experimental data to ensure models are accurate and applicable. However, the simulations and experiments in the paper served different purposes and did not replicate each other. The setups for the simulation model and the experimental tests were not the same, and the measurements were also conducted differently. For example, in the thermal test, the physical experiment used 750ml of water at 50°C as the heat source, with digital thermometers placed in the middle of the water to measure the temperature drop over 30 minutes. In contrast, the simulation model assumed only the top surface of the midsole started at 50°C and measured points at the top surface during a 10-second cooldown. Similarly, in the compression test, only the heel zone was printed and tested in the physical experiment. We considered validation less necessary because the simulation models used were straightforward and widely accepted. Furthermore, the simulation results were intended to offer guidance for optimization rather than for critical use.

Nevertheless, despite the absence of a direct comparison between the results, we have extracted some simulation data as close to the experiment as possible to generate insights. For the thermal simulation, we exported the temperatures of midsole 1 in Fig. 14 after 30 minutes, as shown in Fig. 16a. Due to the aforementioned differences in the heat source, the experimental result showed a slower cooldown rate and thus a higher temperature (40.6°C) than the simulation (35.44°C). Even though the results are not identical, they show sufficient alignment for our purposes. For the compression test, we extracted the deformation only at the heel zone, as shown in Fig. 16b. Under a

similar load as in Fig. 15 with the PLA material, the maximum deformation is 4.44mm, which is very close to the experimental result of 4.35mm. These results indicate that applying simulation is suitable for the solution search process.

6 Conclusion

A new approach for designing custom shoe midsoles using diversity-enhanced swarm intelligence is presented in this paper. The method simultaneously optimizes four independent objectives: plantar stress redistribution, heat dissipation, manufacturability, and aesthetics, using a swarm optimization algorithm to vary the tetrahedral parameters and obtain diverse lattice structures. The diversity of these structures is validated and the method is shown to not only achieve better results for a specific objective but also strike a balance between them to achieve an overall optimal structure. Experimental tests demonstrate that the lattice structure generated by our method outperforms other lattice structures.

Although the present method has shown promise, there are some limitations that need to be addressed. Firstly, the input mesh of the design domain remains fixed during optimization. While the tetrahedral mesh generation can make some changes to the surface mesh, they are not significant. To overcome this, our future work involves adaptively refining the mesh based on high and low stress areas, with the aim of further reducing stress. Secondly, the stress analysis only applied a uniform load to the top surface of the midsole, which may not accurately represent real-world usage. Future work will apply plantar pressure distribution-driven approaches [Cheng et al., 2022] to improve effectiveness. Thirdly, the stress analysis only considered linear material properties, whereas flexible materials exhibit non-linear behavior. To address this, a surrogate model will be developed to capture non-linear properties without compromising computational speed. Additionally, while this paper developed quantitative measurements for four objectives, there are many other objectives for shoe midsoles, such as vibration and energy transfer. Future work will expand to include these objectives. Furthermore, we have only tested one specific set of weights in the optimization process. Future work will involve changing the group of weights to observe their influence on the optimized design. Exploring the impact of different weight configurations on the optimization results could provide valuable insights and enhance the robustness of the findings. Lastly, since the core of our work relies on the PSO algorithm, which balances exploration and exploitation, its effectiveness in finding global optima depends on several factors, including parameter choices, search space complexity, and particle initialization. In practice, PSO can sometimes get trapped in local optima, especially in complex or multimodal search spaces. To mitigate this, various strategies can be employed to enhance PSO's robustness in navigating search spaces and improving its ability to find global optima. These strategies include random restarts, hybrid approaches combining PSO with other optimization techniques (such as simulated annealing), and adaptive techniques that adjust parameters dynamically.

Conflict of interest statement. On behalf of all authors, the corresponding author states that there is no conflict of interest.

Replication of results. The data will be made online available at http://bit.ly/tszhokwok.

Appendix A   Sensitivity Analysis

To avoid long computation times, we should limit our exploration of tetrahedral parameter values to effective ranges that result in distinct structures. In order to identify these ranges, we have conducted a sensitivity analysis by systematically varying one parameter at a time while keeping the others at reasonable values, and observing how the solutions change. To determine these reasonable values, our preliminary analysis tested various settings, and we selected the most representative cases depicted in Fig. A1. This analysis has utilized the manufacturing index (O_M), which is a geometry factor that can be efficiently computed. However, it is important to note that this preliminary analysis is only intended to quickly narrow down the ranges, and is not sufficient for
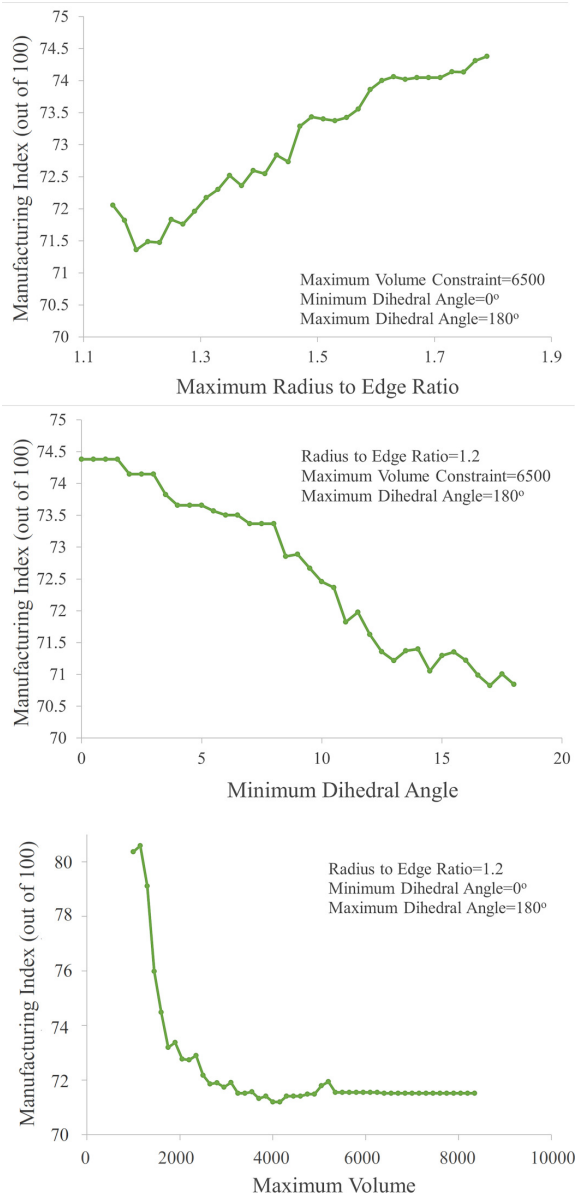
Fig. A1 Sensitivity analysis for three tetrahedral parameters: the maximum radius-to-edge ratio, the minimum dihedral angle, and the maximum volume.

eliminating all duplicate solutions. In this paper, the solutions are generated using three tetrahedral parameters: the maximum radius-to-edge ratio (ρ_{max}), the minimum dihedral angle (φ_{min}), and the maximum volume (V_{max}). For the maximum radius-to-edge ratio, any value below 1.15 fails to generate a mesh, while changes after 1.6 have minimal impact. Therefore, we use 1.15 as

the lower bound and 1.6 as the upper bound, resulting in a range of [1.15 1.6] for this parameter. Regarding the minimum dihedral angle, the analysis shows that values above 18° result in a failure to generate a mesh, while values below this threshold work very well. Hence, the range of the minimum dihedral angle is [0° 18°]. Finally, the maximum volume parameter was found to have a lower bound of 1000 mm^3, as structures generated with smaller volumes have too many thin struts that cannot be fabricated for the required midsole density. Although the maximum volume parameter produces the most variations at smaller values, other parameters have a more significant impact when the maximum volume is higher. For instance, the selected representative cases for the maximum radius to edge ratio and the minimum dihedral angles have a maximum volume of 6500 mm^3. Therefore, we allowed a slight margin and set the upper bound at 7000 mm^3. Thus, the range of the maximum volume is [1000 7000] mm^3

References

[Actis et al., 2008] Actis, R. L., Ventura, L. B., Lott, D. J., Smith, K. E., Commean, P. K., Hastings, M. K., and Mueller, M. J. (2008). Multi-plug insole design to reduce peak plantar pressure on the diabetic foot during walking. *Med. Biol. Eng. Comput.*, 46(4):363–371.

[Aguirre et al., 2020] Aguirre, T. G., Fuller, L., Ingrole, A., Seek, T. W., Wheatley, B. B., Steineman, B. D., Donahue, T. L. H., and Donahue, S. W. (2020). Bioinspired material architectures from bighorn sheep horncore velar bone for impact loading applications. *Scientific Reports*, 10(1):1–14.

[Agwu et al., 2021] Agwu, U. O., Wang, K., Singh, C., Leemhuis, C., Yamakawa, S., and Shimada, K. (2021). Assessing tetrahedral lattice parameters for engineering applications through finite element analysis. *3D Printing and Additive Manufacturing*, 8(4):238–252.

[Ali et al., 2020] Ali, M., Nazir, A., and Jeng, J.-Y. (2020). Mechanical performance of additive manufactured shoe midsole designed using variable-dimension helical springs. *The International Journal of Advanced Manufacturing Technology*, 111(11):3273–3292.

[Armanfar and Gunpinar, 2022] Armanfar, A. and Gunpinar, E. (2022). G-lattices: A novel

lattice structure and its generative synthesis under additive manufacturing constraints. *Journal of Mechanical Design*, pages 1–20.

[Beloshenko et al., 2021] Beloshenko, V., Beygelzimer, Y., Chishko, V., Savchenko, B., Sova, N., Verbylo, D., Voznyak, A., and Vozniak, I. (2021). Mechanical properties of flexible tpu-based 3d printed lattice structures: Role of lattice cut direction and architecture. *Polymers*, 13(17):2986.

[Bielefeldt et al., 2019] Bielefeldt, B. R., Reich, G. W., Beran, P. S., and Hartl, D. J. (2019). Development and validation of a genetic l-system programming framework for topology optimization of multifunctional structures. *Computers & Structures*, 218:152–169.

[Brennan-Craddock, 2011] Brennan-Craddock, J. (2011). *The investigation of a method to generate conformal lattice structures for additive manufacturing*. PhD thesis, Loughborough University.

[Bugin et al., 2020] Bugin, L. A. K., Fagundes, C. V. M., Bruscato, U. M., and Cândido, L. H. A. (2020). Exploration of data-driven midsole algorithm design based in biomechanics data and voronoi 3d to digital manufacturing. *Design e Tecnologia*, 10(21):01–10.

[Cheng et al., 2022] Cheng, H., Liu, B., Liu, M., and Cao, W. (2022). Design of three-dimensional voronoi strut midsoles driven by plantar pressure distribution. *Journal of Computational Design and Engineering*, 9(4):1410–1429.

[Deshpande et al., 2001a] Deshpande, V., Ashby, M., and Fleck, N. (2001a). Foam topology: bending versus stretching dominated architectures. *Acta materialia*, 49(6):1035–1040.

[Deshpande et al., 2001b] Deshpande, V., Fleck, N., and Ashby, M. (2001b). Effective properties of the octet-truss lattice material. *Journal of the Mechanics and Physics of Solids*, 49(8):1747–1769.

[Dessing et al., 2014] Dessing, O., Jansen, A. J., Leihitu, C., and Overhage, D. (2014). Experimental study of heat dissipation in indoor sports shoes. *Procedia Engineering*, 72:575–580.

[Dong et al., 2017] Dong, G., Tang, Y., and Zhao, Y. F. (2017). A survey of modeling of lattice structures fabricated by additive manufacturing. *Journal of Mechanical Design*, 139(10):100906.

[Dong et al., 2019] Dong, G., Tessier, D., and Zhao, Y. F. (2019). Design of shoe soles using lattice structures fabricated by additive manufacturing. *Proceedings of the Design Society: International Conference on Engineering Design*, 1(1):719–728.

[Dong et al., 2018] Dong, G., Wijaya, G., Tang, Y., and Zhao, Y. F. (2018). Optimizing process parameters of fused deposition modeling by taguchi method for the fabrication of lattice structures. *Additive Manufacturing*, 19:62–72.

[El Bouzouiki et al., 2021] El Bouzouiki, M., Sedaghati, R., and Stiharu, I. (2021). A non-uniform cellular automata framework for topology and sizing optimization of truss structures subjected to stress and displacement constraints. *Computers & Structures*, 242:106394.

[Felkner et al., 2013] Felkner, J., Chatzi, E., and Kotnik, T. (2013). Interactive particle swarm optimization for the architectural design of truss structures. In *2013 IEEE Symposium on Computational Intelligence for Engineering Solutions (CIES)*, pages 15–22. IEEE.

[Feng et al., 2021] Feng, J., Liu, B., Lin, Z., and Fu, J. (2021). Isotropic octet-truss lattice structure design and anisotropy control strategies for implant application. *Materials & Design*, 203:109595.

[Guerra Silva et al., 2021] Guerra Silva, R., Torres, M. J., Zahr Viñuela, J., and Zamora, A. G. (2021). Manufacturing and characterization of 3d miniature polymer lattice structures using fused filament fabrication. *Polymers*, 13(4):635.

[Hang, 2015] Hang, S. (2015). Tetgen, a delaunay-based quality tetrahedral mesh generator. *ACM Trans. Math. Softw*, 41(2):11.

[Jones, 2009] Jones, L. (2009). Thermal touch. *Scholarpedia*, 4(5):7955. revision #150165.

[KevinRoot Medical,] KevinRoot Medical. Foot ID. Accessed: 2023-02-25.

[Kinoshita and Bates, 1996] Kinoshita, H. and Bates, B. T. (1996). The effect of environmental temperature on the properties of running shoes. *Journal of applied biomechanics*, 12(2).

[Kwok, 2022] Kwok, T. H. (2022). Improving the diversity of topology-optimized designs by swarm intelligence. *Structural and Multidisciplinary Optimization*, 65(7):202.

19

[Lee and Han, 2022] Lee, Y.-C. and Han, W. (2022). Soccer shoe recommendation system based on multitechnology integration for digital transformation. *Advanced Engineering Informatics*, 51:101457.

[Lei et al., 2019] Lei, H., Li, C., Meng, J., Zhou, H., Liu, Y., Zhang, X., Wang, P., and Fang, D. (2019). Evaluation of compressive properties of slm-fabricated multi-layer lattice structures by experimental test and μ-ct-based finite element analysis. *Mater. Des.*, 169:107685.

[Martínez et al., 2017] Martínez, J., Song, H., Dumas, J., and Lefebvre, S. (2017). Orthotropic k-nearest foams for additive manufacturing. *ACM Transactions on Graphics (TOG)*, 36(4):1–12.

[Muthu and Li, 2021] Muthu, S. S. and Li, Y. (2021). The environmental impact of footwear and footwear materials. *Handbook of footwear design and manufacture*, pages 305–320.

[Nandikolla et al., 2017] Nandikolla, V. K., Bochen, R., Meza, S., and Garcia, A. (2017). Experimental gait analysis to study stress distribution of the human foot. *Journal of medical engineering*, 2017.

[Ning et al., 2022] Ning, K., Yick, K.-L., Yu, A., and Yip, J. (2022). Effects of textile-fabricated insole on foot skin temperature and humidity for enhancing footwear thermal comfort. *Appl. Ergon.*, 104:103803.

[Panetta et al., 2015] Panetta, J., Zhou, Q., Malomo, L., Pietroni, N., Cignoni, P., and Zorin, D. (2015). Elastic textures for additive fabrication. *ACM Transactions on Graphics (TOG)*, 34(4):1–12.

[Rebay et al., 2007] Rebay, M., Arfaoui, A., Leopol, A., Perin, J., and Taiar, R. (2007). Heat transfer in athletic shoes during the running. In Sohrab, S. H., editor, *the 5th IASME/WSEAS International Conference on Heat Transfer, Thermal Engineering and Environment*, Athens, Greece.

[Shimazaki and Aisaka, 2018] Shimazaki, Y. and Aisaka, K. (2018). Novel thermal analysis model of the foot-shoe sole interface during gait motion. *Multidisciplinary Digital Publishing Institute Proceedings*, 2(6):278.

[Sultana et al., 2021] Sultana, A., Kwok, T.-H., and Ng, H. D. (2021). Numerical assessment of directional energy performance for 3d printed midsole structures. *Math. Biosci. Eng.*,

18(4):4429–4449.

[Tang et al., 2021] Tang, Y., Dong, G., Xiong, Y., and Wang, Q. (2021). Data-driven design of customized porous lattice sole fabricated by additive manufacturing. *Procedia Manufacturing*, 53:318–326.

[Tomei et al., 2022] Tomei, V., Faiella, D., Cascone, F., and Mele, E. (2022). Structural grammar for design optimization of grid shell structures and diagrid tall buildings. *Automation in Construction*, 143:104588.

[ul Haq et al., 2022] ul Haq, M. R., Nazir, A., Lin, S.-C., and Jeng, J.-Y. (2022). Design and performance evaluation of multifunctional midsole using functionally gradient wave springs produced using multijet fusion additive manufacturing process. *Mater. Today Commun.*, 31:103505.

[Vaissier et al., 2019] Vaissier, B., Pernot, J.-P., Chougrani, L., and Véron, P. (2019). Genetic-algorithm based framework for lattice support structure optimization in additive manufacturing. *Computer-Aided Design*, 110:11–23.

[Wang et al., 2021] Wang, C., Liu, X., Yue, Y., Huang, J., Huang, X., and Liu, B. (2021). Study on vibration damping mechanism of shoe sole with alternating lattice structure using vibration level difference. *Mathematical Problems in Engineering*, 2021.

[Watson et al., 2022] Watson, M., Leary, M., and Brandt, M. (2022). Generative design of truss systems by the integration of topology and shape optimisation. *The International Journal of Advanced Manufacturing Technology*, 118(3):1165–1182.

[Wu et al., 2019] Wu, J., Wang, W., and Gao, X. (2019). Design and optimization of conforming lattice structures. *IEEE transactions on visualization and computer graphics*, 27(1):43–56.

[Xiao et al., 2022] Xiao, Y., Hu, D., Zhang, Z., Pei, B., Wu, X., and Lin, P. (2022). A 3d-printed sole design bioinspired by cat paw pad and triply periodic minimal surface for improving paratrooper landing protection. *Polymers*, 14(16):3270.

[Yick et al., 2019] Yick, K.-l., Yu, A., and Li, P.-l. (2019). Insights into footwear preferences and insole design to improve thermal environment of footwear. *International Journal of Fashion Design, Technology and Education*, 12(3):325–334.

[Zhang et al., 2020] Zhang, Y., Wang, Z., Zhang, Y., Gomes, S., and Bernard, A. (2020). Bio-inspired generative design for support structure generation and optimization in additive manufacturing (am). *CIRP Annals*, 69(1):117–120.

[Zimmermann et al., 2018] Zimmermann, L., Chen, T., and Shea, K. (2018). A 3d, performance-driven generative design framework: automating the link from a 3d spatial grammar interpreter to structural finite element analysis and stochastic optimization. *AI EDAM*, 32(2):189–199.

[Zolfagharian et al., 2021] Zolfagharian, A., Lakhi, M., Ranjbar, S., and Bodaghi, M. (2021). Custom shoe sole design and modeling toward 3d printing. *International Journal of Bioprinting*, 7(4).